Available online at www.sciencedirect.com

ScienceDirect

Procedia Structural Integrity 42 (2022) 1376–1381

Structural Integrity Procedia

www.elsevier.com/locate/procedia

23 European Conference on Fracture - ECF23

Crack path direction in plane-strain fracture toughness assessment tests of quasi-brittle PLA polymer and ductile PLA-X composite

Aleksa Milovanović[a,*], Miloš Milošević[a], Isaak Trajković[a], Aleksandar Sedmak[b], Mohammad Javad Razavi[c], Filippo Berto[c]

[a]*University of Belgrade, Innovation Center of The Faculty of Mechanical Engineering, Kraljice Marije 16 street, Belgrade 11120, Serbia*
[b]*University of Belgrade, Faculty of Mechanical Engineering, Kraljice Marije 16 street, Belgrade 11120, Serbia*
[c]*Norwegian University of Science and Technology (NTNU), Richard Birkelands vei 2b, 7491, Trondheim, Norway*

Abstract

Plane-strain fracture toughness is one of the main parameters in linear elastic fracture mechanics and its purpose is to show the material capability to withstand load while having a defect. Main validity aspect for such an assessment is to provide a wide enough crack front to enable plane-strain condition. Nonetheless, in FDM (Fused Deposition Modeling), due to structural anisotropy caused by polymer material properties and Additive Manufacturing (AM) process parameters, more validity aspects must be met. During the plane-strain fracture toughness test a crack must follow a straight line from initiation up to the point of structural failure. Plane-strain fracture toughness assessment is conducted according to the ASTM D5045-14 standard for testing of polymer materials. Tests are performed on SENB (Single Edge Notched Bend) specimens, made from two similar polymer materials: quasi-brittle PLA and ductile PLA-X composite. Specimens are manufactured with four different AM process parameters, i.e., layer height, infill density, printing orientation and one specimen batch was dried before testing.

Keywords: Fracture toughness; PLA polymer; PLA-X composite;

1. Introduction

Fused Deposition Modeling (FDM) Additive Manufacturing (AM) technology is based on material extrusion process where melted plastic is selectively dispensed onto a build platform through a heated nozzle. Nowadays, the most used FDM materials are ABS (Acrylonitrile Butadiene Styrene) and PLA (PolyLactic Acid), according to

* Corresponding author. Tel.: +381-64-614-8698.
E-mail address: amilovanovic@mas.bg.ac.rs

10.1016/j.prostr.2022.12.175

Milovanovic et al. (2020). Clear PLA material advantage over ABS is in high dimensional accuracy (according to Milovanovic et al. (2019)) and biodegradable nature of the material. For the purpose of mechanical property enhancement FDM technology allows for a combination of materials in one filament, addition of second-phase particles or carbon and glass fibers in the material matrix. One such material, so-called ‘’PLA-X’’ (Mitsubishi Chemical, Japan), was a subject of previous research conducted by Milovanovic et al. (2020), for the assessment of material’s tensile properties and results were compared with mechanical properties of pure PLA material, in order to obtain second-phase particle influence on PLA material. Also, in the next research conducted by Milovanovic et al. (2021), the fracture surfaces of PLA and PLA-X materials were observed. Namely, almost all the PLA specimens broke in brittle manner, while PLA-X developed crazing before fracture, which resulted in ductile behavior of the material. Such yielding mechanism, so-called ‘’crazing’’, is described in Anderson (2005).

Continuation of this research is the fracture toughness assessment of both PLA and PLA-X material and crack path direction analysis, using plane-strain fracture toughness test method according to ASTM D5045-14 standard. Mentioned standard covers Compact Tension (CT) and Single Edge Notched Bend (SENB) specimens. In this research, only SENB specimens are printed, with specimen faces parallel to the build platform, as illustrated in Fig. 1.

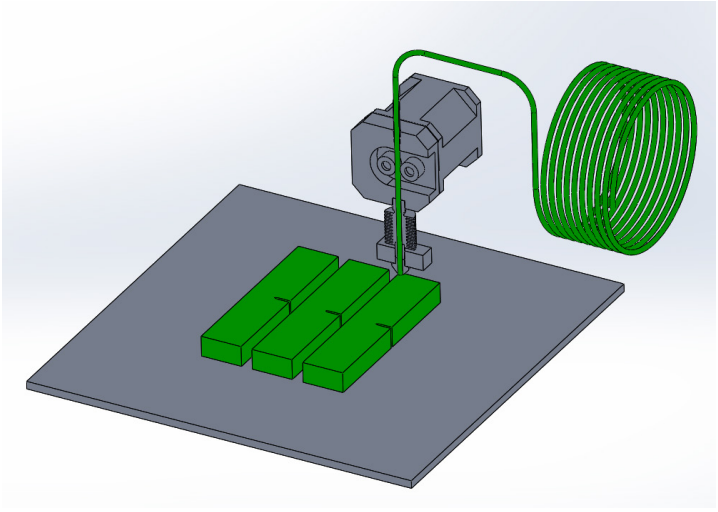

Fig. 1. FDM printing and printing orientation of SENB specimens.

Fracture toughness assessment of AM materials is very common in research literature. Concerning FDM technology, Ayatollahi et al. (2020) conducted research on Semi-Circular Bending (SCB) specimens for Mode I fracture toughness assessment. Regarding tensile tests, also conducted in his research, 0°/90° angle of orientation gave highest UTS results, but in fracture toughness assessment specimens with +45°/-45° angle had highest failure loads and a largest amount of plastic deformation, with properties decreasing toward 0°/90° angle. Research conducted by Park et al. (2006) considered Mode I fracture toughness assessment of PLA material in order to obtain the effect of crystallinity and loading-rate, Pickering et al. (2011) considered fracture toughness tests for the assessment of mechanical behavior of fiber-reinforced PLA bio-composites, Kanakannavar et al. (2020) used fracture toughness tests to compare properties of yarn woven PLA and pure PLA material. Fracture toughness tests are not ‘’strange’’ to other AM technologies: Stoia et al. (2020) used SENB specimens on 3-point bending test fixture for Selective Laser Sintered (SLS) polyamide and alumide materials, Linul et al. (2020) used 4-point bending test fixture to assess Mode I and Mode II of SLS polyamide material. Also, Mode I, Mode II and Mode III and all Mode mixities can be assessed using particular fixture for Compact Tension Shear (CTS) specimens, according to Razavi et al. (2019). This fixture was used for the assessment of PMMA material properties, conducted by Razavi et al. (2019).

According to Valean et al. (2020), effect of notch insertion in the specimen is more evident in Mode I, than in Mode II. Author states that specimens with directly 3D printed notches have less result scatter, than milled ones. Thus, this research will comply with previously mentioned author’s suggestions.

For the assessment of crack path direction, a Digital Image Correlation (DIC) dual-camera set device is used, with dedicated software for data acquisition. DICs are used for AM materials, namely research conducted by Gljuscic et al. (2020), Brugo et al. (2021), Bouaziz et al. (2021). Before use in AM materials, DICs were used for biomaterials: namely Colic et al. (2017), Mitrovic et al. (2019), Miletic et al (2016) and Sedmak et al. (2012); for the assessment of the actual stress-strain diagram of welded joints, with obtained results paired with FEM ones, conducted by Milosevic et al. (2021) and Milosevic et al. (2021); for process equipment: Mitrovic et al. (2018).

Nomenclature

FDM	Fused Deposition Modeling
AM	Additive Manufacturing
ABS	Acrylonitrile Butadiene Styrene
PLA	PolyLactic Acid
CT	Compact Tension
SENB	Single Edge Notched Bend
SCB	Semi- Circular Bending
UTS	Ultimate Tensile Strength
SLS	Selective Laser Sintering
CTS	Compact Tension Shear
PMMA	PolyMethyl MethAcrylate
DIC	Digital Image Correlation
FEM	Finite Element Method

2. Materials and methods

Ten batches of PLA and PLA-X SENB specimens are prepared with five specimens per batch i.e., total of fifty specimens. According to ASTM D5045-14 standard for fracture toughness tests three specimens are mandatory and two other prepared specimens act as replacements if some of the tests fail. SENB specimen batches are prepared with the same printing parameters as the tensile tests conducted by Milovanovic et al. (2020) with variation in layer height, infill density, printing orientation and one batch includes dried specimens. Thus, printing parameters of SENB specimen batches are:

- First batch: 0.1 mm layer height, 50% infill density
- Second batch: 0.1 mm layer height, 100% infill density, rectilinear orientation
- Third batch: 0.1 mm layer height, 100% infill density, circular orientation
- Fourth batch: 0.2 mm layer height, 50% infill density
- Fifth batch: 0.1 mm layer height, 50% infill density, dried specimens before testing

All SENB specimen bulk dimensions are 13x26x114.4 mm, with notch height and width of 10 mm and 1.5 mm, respectively. Notch has a 45° sharp tip, pre-crack is approximately 3 mm long. Pre-crack is created with a hammer tapping onto a sharp razor placed in the notch, according to ASTM D5045-14 standard. Specimens are tested on a universal tensile testing machine with loaded 3-point bending test fixture. Distance between supporting pins is set at 104 mm, supporting pins and loading pin radius is 10 mm. Strain rate is set at 5 mm/min. First calculated fracture toughness value is conditional, and has to meet the plane-strain criterion from the ASTM D5045-14 standard. Due to the limited length of this paper and because the subject is oriented toward crack path direction analysis, the obtained fracture toughness results will be shown in the extended paper.

Central part of each SENB specimen is sprayed with mate paint to obtain better image quality with DIC cameras. Dual-camera set device from the GOM manufacturer (GOM GmbH, Braunschweig, Germany) are used to capture full-field deformation of the front side of each SENB specimen, Fig. 2a. For data acquisition of DIC results dedicated Aramis software (GOM GmbH, Braunschweig, Germany) is used. In the software non-contact strain gauges can be created which can show deformations on the selected section. Here, on every SENB specimen five sections are placed on the ligament, circa 45 mm long (Fig. 2b). As an output of the created section a deformation diagrams are obtained, showing von Mises deformation values along the created sections.

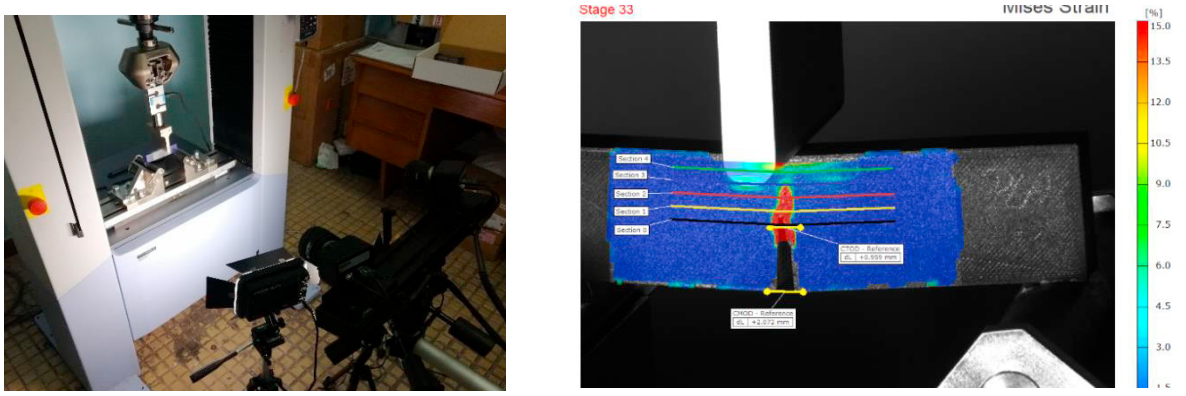

Fig. 2. (a) SENB specimen loaded onto a 3-point bending test fixture on universal testing machine and DIC cameras placed in front to capture the front side of the specimen; (b) image from Aramis software with created sections on specimen ligament.

3. Results and Discussion

Highest average force value in previous tensile tests (conducted by Milovanovic et al. (2020)) are achieved in the third batch which has circular orientation, i.e., where filament lines match the force direction. In fracture toughness tests, the second batch (with rectilinear, +45°/-45° angle, orientation) can withstand the highest loads, which corresponds to the Ayatollahi et al. (2020) research. The concern of this paper are the deformation diagrams, some are shown in Fig. 3. The most noticeable feature in deformation diagrams is the fact that all full infill batches, i.e., second and third batch, have greater von Mises deformation value scatter along created sections (Fig. 3b). Highest deformations are present in the first batch (with 50% infill), with values arranged in ‘’candle shape’’ (Fig. 3a).

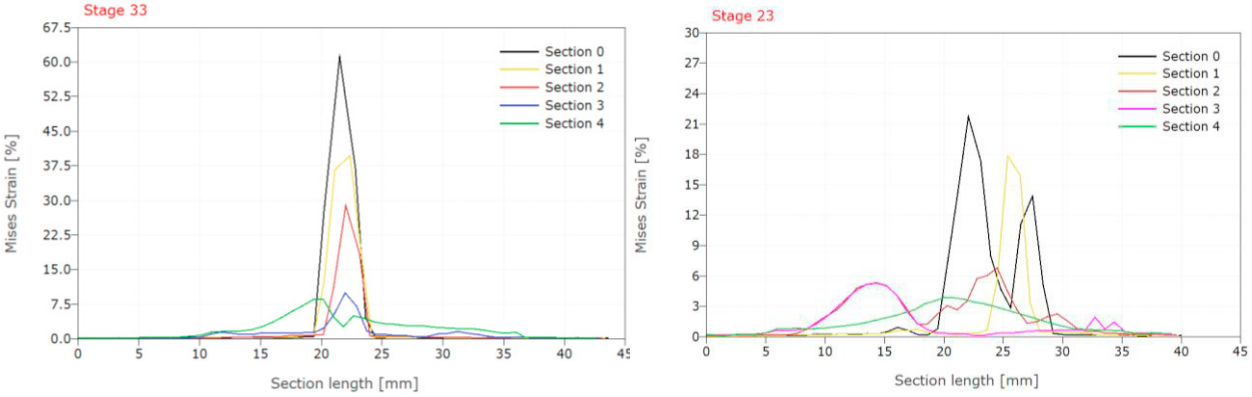

Fig. 3. (a) One deformation diagram from the first batch; (b) third batch.

Previously called ‘’candle shape’’ curves suggest that the highest deformation values are only present at the places of the expected crack path direction, on all selected sections. Hence, showing that the crack propagation will follow a vertically straight path. In other 50% batches, namely fourth and fifth, deformation values don’t follow an ‘’candle shape’’ curve just as the first batch, i.e, deformation values are a bit lower and value scatter is present, but not as in specimens with full infill density. Thus showing that specimen drying and higher layer height have an effect on crack path direction. In higher layer height specimens (0.2 mm), lower bonding in-between layers can cause local stress concentrators in the vicinity of the crack tip, hence creating deformation value scatter. Specimen drying may cause material shrinking toward the center of printed lines, thus weakening bond in-between layers.

Higher scatter of deformation results along section lines may indicate a sudden change in crack direction, different from the expected crack path. As in rectilinear and circular orientation specimens, crack may change the expected direction due to the influence of lower material resistance in-between printed lines, from where a crack may continue to

propagate. This material behaviour is more prone in specimens with higher infill density. Such value scatter may indicate to a certain behaviour in the specimen during the test, such as the creation of stress concentrators in the vicinity of a crack. One such case is noted in the third batch, on both PLA and PLA-X specimens. Third batch has a circular printing orientation i.e., has perpendicular printed lines to particular load direction. On one such specimen we have a section that goes through one stress concentration, Fig. 4a, and have recorded highest strain value of that concentrator (Fig. 4b).

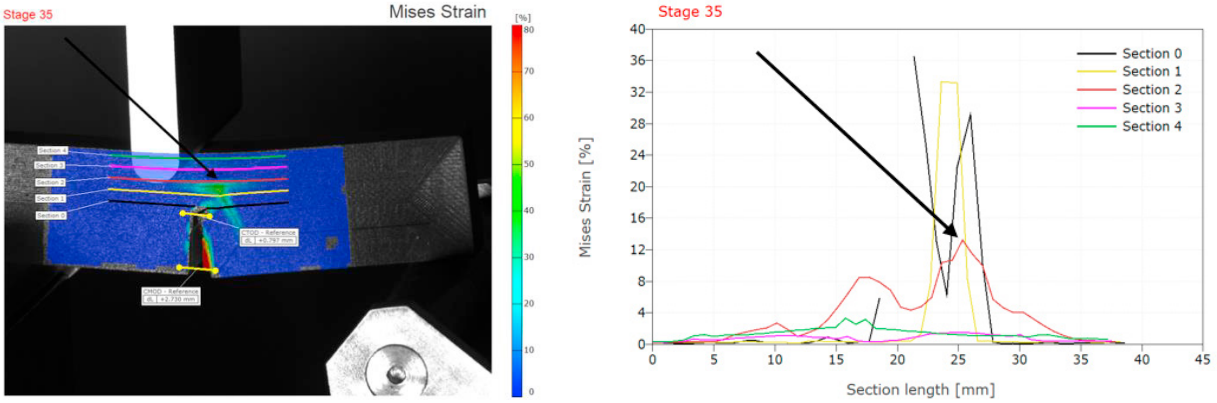

Fig. 4. (a) Stress concentrator on the specimen (shown by the arrow); (b) deformation value of that concentrator (shown by the arrow).

Described stress concentrator also has an effect on Force-displacement (F-l) diagram of fracture toughness tests, changing the F-l curvature slope. The effect of that concentrator is shown with arrows on Fig. 5, for both PLA and PLA-X material. Due to the ductile nature of PLA-X material (Milovanovic et al. (2021)) its F-l curve (Fig. 5b) has a slight curvature slope change, compared to quasi-brittle PLA (Fig. 5a). Such F-l curve slope change points to the fracture toughness test failure, accoring to ASTM D5045-14 standard.

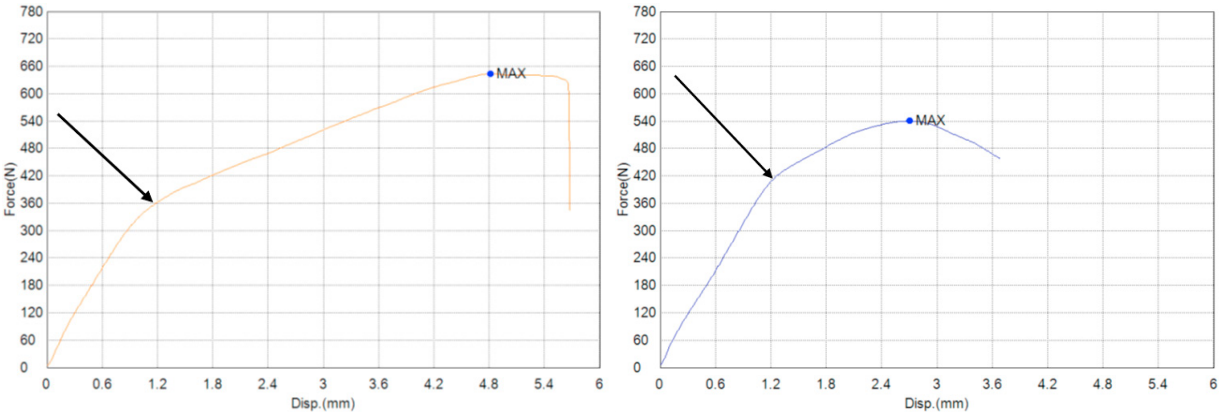

Fig. 5. (a) F-l diagram from the third batch of PLA; (b) PLA-X material.

4. Conclusions

Crack path direction analysis on SENB fracture toughness test specimens using DIC dual-camera set device has shown the following:

- All full infill specimen batches have high deformation value scatter along selected sections (i.e., virtual strain gauges).
- First specimen batch, with 50% infill and 0.1 mm layer height, produced ‘’candle shape’’ curves on deformation diagrams, showing than a crack will certainly propagate following an expected straight direction from pre-crack stage to immanent failure.
- Other 50% infill batches have lower maximum von Mises deformation value and slight value scatter.

- Specimen drying and higher layer height will result in lower bonding in-between layers, allowing for the crack to continue propagation in-between printed lines, thus deviating it from the expected path.
- Deformation data from the selected sections may point to local stress concentrators in the vicinity of the crack, that can influence on crack path direction.
- F-l data from some third batch fracture toughness tests of PLA-X material show minor slope change compared to PLA material, mainly due to material's ductile nature.

Acknowledgements

The authors would like to thank the support from European Union's Horizon 2020 research and innovation program (H2020-WIDESPREAD2018, SIRAMM) under grant agreement No. 857124.

References

Milovanović, A., Sedmak, A., Grbović, A., Golubović, Z., Mladenović, G., Čolić, K., Milošević, M., 2020. Comparative analysis of printing parameters effect on mechanical properties of natural PLA and advanced PLA-X material. Procedia Structural Integrity 28, 1963-1968.

Milovanović, A., Milošević, M., Mladenović, G., Likozar, B., Čolić, K., Mitrović, N., 2019. Experimental Dimensional Accuracy Analysis of Reformer Prototype Models Produced by FDM and SLA 3D Printing Technology. Experimental and Numerical Investigations in Materials Science and Engineering, in: Mitrović, N., Milošević, M., Mladenović, G. (Ed.). Springer, Cham; 84-95.

Milovanović, A., Sedmak, A., Grbović, A., Golubović, Z, Milošević, M., 2021. Influence of second-phase particles on fracture behavior of PLA and advanced PLA-X material. Procedia Structural Integrity 31, 122-126.

Anderson, T.L., 2005. Fracture Mechanics: Fundamentals and Applications, Third Edition, Taylor &Francis Group, 265-268.

Ayatollahi, M.R., Nabavi-Kivi, A., Bahrami, B., Yahya, M.Y., Khosravani, M.R., 2020. The influence of in-plane raster angle on tensile and fracture strengths of 3D-printed PLA specimens. Engineering Fracture Mechanics 237, 107225.

Park, S.D., Todo, M., Arakawa, K., Koganemaru, M., 2006. Effect of crystallinity and loading-rate on mode I fracture behavior of poly (lactic acid). Polymer 47, 1357-1363.

Pickering, K.L., Sawpan, M.A., Jayaraman, J., Fernyhough, A., 2011. Influence of loading rate, alkali fiber treatment and crystallinity on fracture toughness of random short hemp fiber reinforced polylactide bio-composites. Composites: Part A 42, 1148-1156.

Kanakannavar, S., Pitchaimani, J., 2021. Fracture toughness of flax braided yarn woven PLA composites. International Journal of Polymer Analysis and Characterization, 26:4, 364-379.

Stoia, D.I., Marsavina, L., Linul, E., 2020. Mode I Fracture Toughness of Polyamide and Alumide Samples obtained by Selective Laser Sintering Additive Process. Polymers 12, 640.

Linul, E., Marsavina, L., Stoia, D.I., 2020. Mode I and II fracture toughness investigation of Laser-Sintered Polyamide. Theoretical and Applied Fracture Mechanics 106, 102497.

Razavi, S.M.J., Berto, F., 2019. A new fixture for fracture tests under mixed mode I/II/III loading. Fatigue Fract Eng Mater Struct., 1-15.

Razavi, S.M.J., Berto, F., 2019. Mixed mode I/II/III fracture assessment of PMMA using a new test fixture. MATEC Web of Conferences 300, 11003.

Valean, C., Marsavina, L., Marghitas, M., Linul, E., Razavi, J., Berto, F., Brighenti, R., 2020. The effect of crack insertion for FDM printed PLA materials on Mode I and Mode II fracture toughness. Procedia Structural Integrity 28, 1134-1139.

Gljuščić., M., Franulović, M., Lanc, D., Božić, Ž., 2021. Digital image correlation of additively manufactured CFRTP composite systems in static tensile testing. Procedia Structural Integrity 31, 116-121.

Brugo, T.M., Campione, I., Minak, G., 2021. Investigation by Digital Image Correlation of Mixed-Mode I and II Fracture Behavior of Polymeric IASCB Specimens with Additive Manufactured Crack-Like Notch. Materials 14, 1084.

Bouaziz, M.A., Marae-Djouda, J., Zouaoui, M., Gardan, J., Hild, F., 2021. Crack growth measurement and J-integral evaluation of additively manufactured polymer using digital image correlation and FE modeling. Fatigue Fract Eng Mater Struct. 44, 1318-1335.

Čolić, K., Sedmak, A., Legweel, K., Milošević, M., Mitrović, N., Mišković, Ž., Hloch, S., 2017. Experimental and numerical research of mechanical behaviour of titanium alloy hip implant. Technical gazette 24 (3), 709-713.

Mitrović, A., Mitrović, N., Tanasić, I. Milošević, M., Antonović, D., 2019. Strain Field Measurements in Glass Ionomer Cement, Structural Integrity and Life, 19(2), 143-147

Miletić, V., Perić, D., Milošević, M., Manojlović, D., Mitrović, N., 2016. Local deformation fields and marginal integrity of sculptable bulk-fill, low-shrinkage and conventional composites. Dental Materials 32 (11), 1441-1451.

Sedmak, A., Milošević, M., Mitrović, N., Petrović, A., Maneski, T., 2012. Digital image correlation in experimental mechanical analysis, Structural Integrity and Life, 12(1), 39-42

Milošević, N., Sedmak, A., Bakić, G., Lazić, V., Milošević, M., Mladenović, G., Maslarević, A., 2021. Determination of the Actual Stress-Strain Diagram for Undermatching Welded Joint Using DIC and FEM. Materials 14, 4691.

Milošević, N., Sedmak, A., Martić, I. Prokić-Cvetković, R., 2021. Novel procedure to determine actual stress-strain curves, Structural Integrity and Life, 21(1), 37-40,

Mitrović, N., Petrović, A., Milošević, M., 2018. Strain measurement of pressure equipment components using 3D Digital Image Correlation method. Procedia Structural Integrity 13, 1605-1608.